DESIGN AND OPTIMISATION OF A HIGHLY FLEXIBLE WING STRUCTURE FOR A GENERIC LONG-RANGE AIRCRAFT

Markus Zimmer and Kjell Bramsiepe

German Aerospace Center DLR, Institute of Aeroelasticity, Göttingen, Germany Markus.Zimmer@dlr.de, Kjell.Bramsiepe@dlr.de

Abstract

Due to the increased application of carbon fibre reinforced plastics (CFRP) in the aircraft industry in the past decades, design of primary load carrying structures has vastly evolved. Particularly, the Airbus A350 and the Boeing 787 are well known for their complete integral structures fabricated entirely out of CFRP. Ultimately, this led to weight saving and a wider design space as the result of reduced material density and the anisotropic nature of the composite. However, the aforementioned design space is currently limited by uncertainties such as material imperfections, open hole tensions or plate boarder stresses. These uncertainties are commonly overcome by applying large safety margins, limiting the benefit of replacing aluminium with carbon fibre.

This work analyses the impact of increased strain failure limits on the structural optimisation of an aircraft wing structure. The goal is the design of a highly flexible wing box to form the groundwork for further research on the effects of large, geometrically nonlinear deformations in the field of aeroelasticity. Therefore, a parametric, in-house model generator is used to build a research model which features the attributes of a modern long range jet transport. Throughout this paper, simulation model components and topological decisions are presented, as well as the loads and optimisation tool chain which is applied to dimension the structure. The optimisation of the composite skin is based on a lamination parameter methodology in which the shell elements are restricted by strain and intracell buckling constraints. Initial results obtained from geometrically nonlinear finite element calculations with varying static manoeuvre loads indicate that the optimised structure is suffering from buckling of whole stiffed panels. As a consequence, responses obtained by linear buckling analyses are considered in the optimisation as well. Finally, the results of a parameter variation are presented. The generated structural model features a vertical wing tip displacement of 8.6% with respect to the wing half span during design cruise flight. Furthermore, the usability of the optimisation results for geometrically nonlinear calculations is demonstrated.

1. INTRODUCTION

In a time of increased awareness of climate changes and protests for political action going around the world [1], aircraft manufactures are more than ever admonished to intensify their efforts to increase the efficiency of their fleet. One key instrument with the potential of reducing the consumption of fossil fuels is the application of anisotropic materials like carbon fibre reinforced plastics (CFRP). Composite materials allow for tailoring of structural stiffness for specific demands, reducing unnecessary weight. However, the potential benefits of utilising anisotropic materials are rarely maxed out, as uncertainties in the design process of CFRP require the large safety margins. Therefore, the presented work aims to analyse the impact of increased strain limits onto the design process of aircraft wing structures.

The groundwork for the demonstrated research was laid in the project ATLAS²Hybrid [2], as part of the Luftfahrtforschungsprogramm (LuFo). Goal of the work

package AP2340 was to design a wing box structure of a long range jet transport featuring 10 % vertical wing tip displacement with respect to half span during cruise flight. This structure was determined to feature key aspects of a realistic stiffened shell structure. After the end of the project in 2018, the research was continue in order to generate a simulation model for further aeroelastic investigations on the subject of large deformations.

The overall design process may be divided into 4 major segments. At first, the definition of the key aircraft attributes are illustrated, followed by an overview of the prepared simulation models used for loads generation and structural optimisation. Furthermore, the tool chain is presented, automating the complete design process. Lastly, the results of a parameter variation are discussed, along with geometrically nonlinear finite element calculations carried out to verify the integrity and usability of the optimised structural model.

2. AIRCRAFT CHARACTERISTICS

In order to maximise the potential flexibility of the aircraft wing structure, a modern long rang jet transport is designed, featuring attributes comparable to the Airbus A350 and a Boeing 787. Consequently, a set of aircraft parameters are defined as listed in Table 1. The design conditions of the aircraft are defined to be at a Mach number of 0.85 at an elevation of 35000 ft.

| Aircraft Parameter Definitions | |
|--------------------------------|----------------------|
| range | 15000 km |
| MTOW | 275.0 t |
| span | 65.0 m |
| length | 67.0 m |
| PAX | 332 |
| Mmo | 0.89 |
| fuel capacity | 115.0 t |
| reference surface | 445.0 m ² |
| aspect ratio | 9.40 |
| MAC | 9.0 m |

Table 1: General Aircraft Specifications

Based on these characteristics, several mass distributions are derived. Multiple loading states – empty, zero fuel and maximum take off mass – are combined with varying distributions to create the envelope depicted in Figure 1.

In accordance with CS25, a flight envelope as shown in Figure 2 is generated. For this purpose, stall and manoeuvre speeds are estimated for all mass distributions in compliance with European flight regulations [3].

To respect the dependency of stall speeds on to the maximum lift coefficient (cL_{max}), a correlation between cL_{max} and the Mach number (Ma) is estimated based on geometrical aspects of the wing as shown in [4]. The resulting trend is handed over to a regression algorithm determining the stall speed slopes.

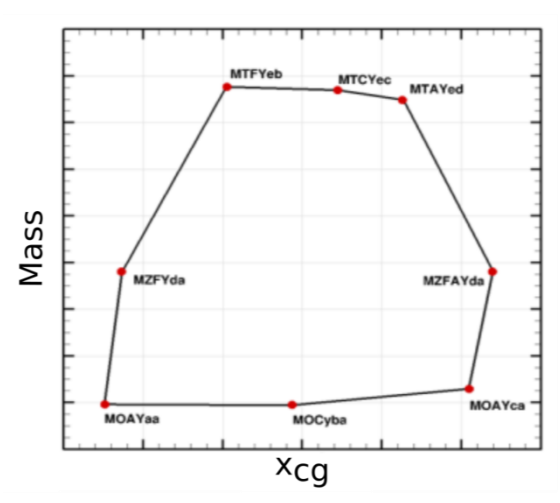


Figure 1: Mass Cases

Based on this flight envelope, three static manoeuvres (see CS 25.30 and following) are chosen for loads generation: a 2.5g pull up, -1.0g push down and an accelerated roll manoeuvre. The generated loads are used in the context of the structural optimisation phase.

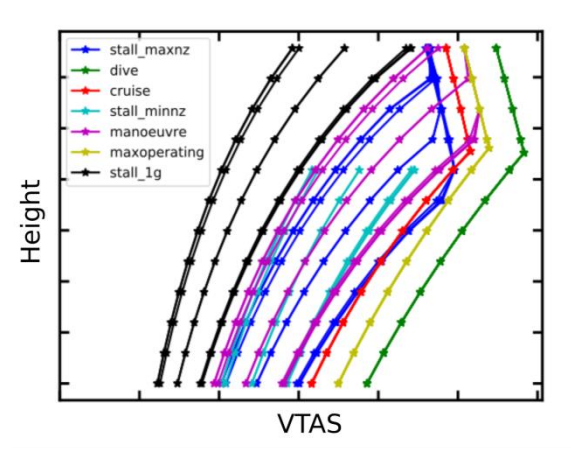


Figure 2: Flight Envelope, Design and Manoeuvre Speeds

3. SIMULATION MODEL COMPONENTS

All parts of the presented simulation model are generated by means of the in-house model generator ModGen. Its parametric approach allows for simple and fast adjustments of the simulation model as a whole. The capabilities of ModGen are presented in detail in [5]. The necessary components for generation of manoeuvre loads and structural optimisation are described in the following.

3.1. Structure

The structural finite element model, as depicted in Figure 3 features all necessary elements needed for aeroelastic manoeuvre calculations. Fuselage and pylons are represented by beam elements, dimensioned using sizing methodologies typically utilised in a conceptual design phase. The engine cowlings are rigid and may be used for mass integration and fluid-structure-coupling. All components which are highlighted in purple constitute rigid structures being used for splining purposes, with one exception being the central wing attachment. In accordance with [6], this attachment distributes various degrees of freedom of the model clamping to several ribs of the central wing box. To a certain extend, this methodology resembles the integration of the wing into the fuselage.

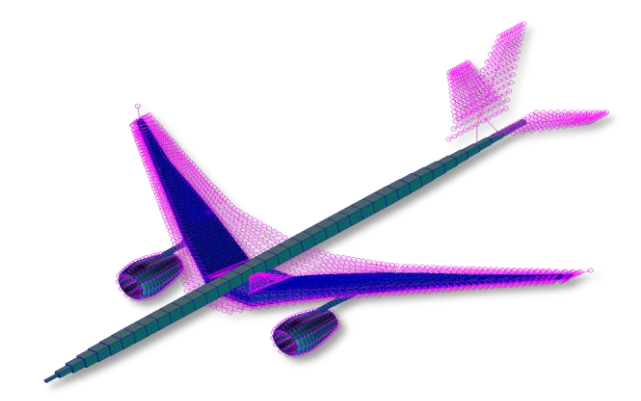


Figure 3: Structural Model with Fluid-Structure-Coupling Elements

A sectional view of the aforementioned wing box is presented in f. Its structure is modelled as a stiffened shell construction and is composed out of upper and lower skin, ribs, as well as three spars, with the middle spar ending shortly after the engine. All elements are modelled out of CFRP composites. The design process of the material properties is illustrated in chapter 3.4.

As buckling is expected to be the main restriction during the optimisation of highly flexible structures, the distance between stiffening structures is considerably decreased. The latter is achieved by increasing the number of skin stiffening stringers to 30 and the count of ribs to 53.

Consequently, it becomes necessary to model the stringer elements to terminate in the vicinity of spars, instead of continuing the stiffener until the wing tip. This, however, increases the complexity of the discretisation procedure.

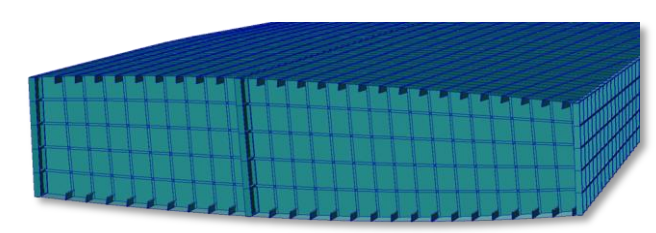


Figure 4: Sectional View of Wing Box Structure

Despite considerable simplifications, like the lack of man holes and attachments structures of high lift devices, the finite element model of the load carrying wing box structure is expected to be of reasonable accuracy in the context of a preliminary design phase.

3.2. Mass

The mass model is composed out of various components as visible in Figure 5. Primary structural components such as fuselage, tail planes, engines or landing gear, as well as the payload are estimated based on similar designs and integrated as point masses. Secondary structural masses, corresponding high lift devices, wing tips, attachments, rivets and paint, are estimated based on semi-empirical approaches taken from [7] and [8]. Thereafter, those components are modelled in ModGen as a simplified structure, featuring the estimated mass. Finally, these structures are condensed section wise to point masses. This procedure provides an estimate for the mass moment of inertia of these components.

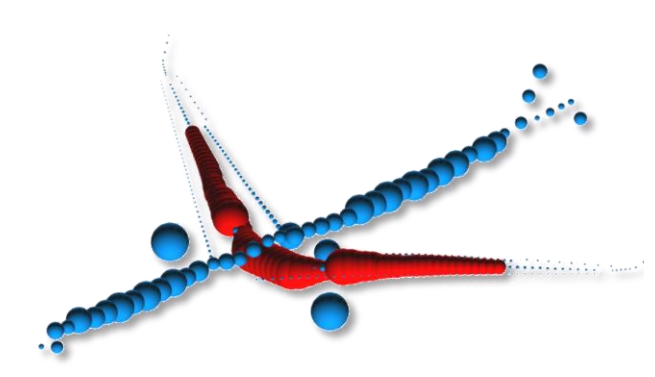


Figure 5: Mass Visualisation, Payload and Structural Components not being Focus of Optimisation (blue), Fuel (red)

In order to estimate a meaningful fuel mass distribution, a fuelling sequence is derived based on the internal volume of the wing box. As the wing features two separate fuel tanks, this sequence is designed in a way that the outer fuel tank is filled completely before the inner one is fuelled. During flight this procedure is reversed to retain as much fuel in the wing's most outer tank, acting against the lifting forces and reducing the wing bending moment.

As the mass of the wing box changes during the optimisation, trim masses are generated to retain the total mass and the centre of gravity of each individual mass case. The masses are consequently added as additional payload.

3.3. Aerodynamics

Aerodynamic calculations are carried out by means of the vortex lattice method implemented in MSC.NASTRAN. Therefore, the aerodynamic model depicted in Figure 6 features a panel based discretisation. The fuselage, however, is represented by a slender body.

In order to account for camber and twist aspects, a W2GJ correction is utilised [9], adjusting the normal vector of the individual panels. All main control surfaces may be addressed during trim simulations.



Figure 6: Panel Based Aerodynamic Representation

3.4. Optimisation

Structural optimisation calculations of the presented wing box are carried out using the gradient based interior point method (IPOPT) [10] embedded in MSC.NASTRAN SOL200. Throughout adjusting material and element based properties, the optimiser seeks an optimum to an objective function. Current industry standard is to minimise the mass of the primary load carrying structure (eq. (1)). However, mass constitutes a wage objective, since its optimum may be determined throughout numerous different combinations of properties. Moreover, as the structures become more flexible, it is potentially beneficial to consider additional information related to the deformation of the wing in order to enforce a certain tendency of the design. One approach is to maximise the vertical displacement of the wingtip $\Delta t_{3,wt}$ (eq. (2)). A combination of the two functions can be achieved by minimising a weighted function in the form of the primary mass divided by the $\Delta t_{3,wt}$. Thereby, the mass of the wing is minimised while the wing bending is maximised. One downside of this approach is that the optimum constitutes a Pareto-surface, meaning the optimisation may result in a lighter or more flexible wing, while obtaining the same objective value. The latter can be manipulated by assigning different exponents (φ,ζ) to the particular elements of the function, altering the gradient of the objective (eq. (3)).

$$f(X_{DV}) = \min(\text{mass}) \tag{1}$$

$$f(\mathbf{X}_{DV}) = \max(\Delta t_{3,wt}) \tag{2}$$

$$f(\mathbf{X}_{DV}) = \min\left(\frac{mass^{\varphi}}{\Delta t_{3wt}^{\zeta}}\right)$$
 (3)

The individual components of the optimisation model, its design variables and optimisation constraints are discussed in further detail below.

3.4.1. Lamination Parameters

Following the classical laminate theory, the elastic characteristics of composite materials may be approximated by equations (4) and (5). These equations relate the laminate strains to the stresses along the edges of a shell element by defining the extensional stiffness matrix A, the coupling stiffness matrix B, and the bending stiffness matrix D.

$$\begin{bmatrix} N_{x} \\ N_{y} \\ N_{xy} \end{bmatrix} = \mathbf{A} \begin{bmatrix} \epsilon_{x}^{0} \\ \epsilon_{y}^{0} \\ \gamma_{xy}^{0} \end{bmatrix} + \mathbf{B} \begin{bmatrix} \kappa_{x} \\ \kappa_{y} \\ \kappa_{xy} \end{bmatrix}$$
(4)

$$\begin{bmatrix} M_{x} \\ M_{y} \\ M_{xy} \end{bmatrix} = \mathbf{B} \begin{bmatrix} \epsilon_{x}^{0} \\ \epsilon_{y}^{0} \\ \gamma_{xy}^{0} \end{bmatrix} + \mathbf{D} \begin{bmatrix} \kappa_{x} \\ \kappa_{y} \\ \kappa_{xy} \end{bmatrix}$$
 (5)

In order to describe these matrices without the definitions of specific stacking of laminates, Tsai and Pegano introduced so-called lamination parameters V [11]:

$$(V_{1A}, V_{2A}, V_{3A}, V_{4A}) = \frac{1}{h} \int_{-h/2}^{h/2} (\cos 2\Theta, \sin 2\Theta, \cos 4\Theta, \sin 4\Theta) dz, \tag{6}$$

$$(V_{1B}, V_{2B}, V_{3B}, V_{4B}) = \frac{4}{h^2} \int_{-h/2}^{h/2} z(\cos 2\Theta, \sin 2\Theta, \cos 4\Theta, \sin 4\Theta) dz,$$
 (7)

$$(V_{1D}, V_{2D}, V_{3D}, V_{4D}) = \frac{12}{h^3} \int_{-h/L}^{h/2} z^2(\cos 2\Theta, \sin 2\Theta, \cos 4\Theta, \sin 4\Theta) dz.$$
 (8)

These 12 parameters factorise the material invariant matrices Γ to compose the individual stiffness matrices:

$$\mathbf{A} = \mathbf{h}(\mathbf{\Gamma}_0 + \mathbf{\Gamma}_1 V_{1A} + \mathbf{\Gamma}_2 V_{2A} + \mathbf{\Gamma}_3 V_{3A} + \mathbf{\Gamma}_4 V_{4A}),\tag{9}$$

$$\mathbf{B} = \frac{4}{h^2} (\mathbf{\Gamma}_1 V_{1B} + \mathbf{\Gamma}_2 V_{2B} + \mathbf{\Gamma}_3 V_{3B} + \mathbf{\Gamma}_4 V_{4B}), \tag{10}$$

$$\mathbf{D} = \frac{h^3}{12} (\mathbf{\Gamma}_0 + \mathbf{\Gamma}_1 V_{1D} + \mathbf{\Gamma}_2 V_{2D} + \mathbf{\Gamma}_3 V_{3D} + \mathbf{\Gamma}_{4D}). \tag{11}$$

The matrices Γ_0 - Γ_5 comprise the material invariants U, which only depend on the material properties of a single ply: For further reading please refer to [11]. The descried methodology is integrated into NASTRAN via the specifications of user functions. This way the calculation of sensitivities is carried out by NASTRAN itself.

$$\Gamma_{0} = \begin{bmatrix} U_{1} & U_{4} & 0 \\ U_{4} & U_{1} & 0 \\ 0 & 0 & U_{5} \end{bmatrix}, \Gamma_{1} = \begin{bmatrix} U_{2} & 0 & 0 \\ 0 & -U_{2} & 0 \\ 0 & 0 & 0 \end{bmatrix}, \Gamma_{2} = \frac{1}{2} \begin{bmatrix} 0 & 0 & U_{2} \\ 0 & 0 & U_{2} \\ U_{2} & U_{2} & 0 \end{bmatrix},$$

$$\Gamma_{3} = \begin{bmatrix} U_{3} & -U_{3} & 0 \\ -U_{3} & U_{3} & 0 \\ 0 & 0 & -U_{3} \end{bmatrix}, \Gamma_{4} = \begin{bmatrix} 0 & 0 & U_{3} \\ 0 & 0 & -U_{3} \\ U_{3} & -U_{3} & 0 \end{bmatrix}.$$
(12)

3.4.2. Shell Elements

Based on the previously illustrated lamination parameters, an optimisation model for the planar elements of the wing box structure is derived. The structure is divided into 117 design domains as indicated by the colouring in Figure 7. In the context of the presented work, lamination parameters are formulated in such a way that they describe an unbalanced symmetric laminate.

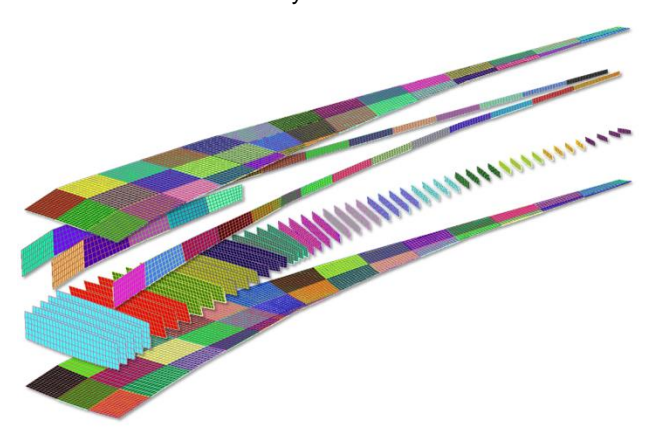


Figure 7: Visual Representation of Design Domains, Plate Elements

Due to the symmetric composition of the laminate, the matrix **B** in equations (4) and (10) becomes equal to zero and the amount of parameters is reduced from 12 to 8. Following [12] and [13], compatibility constraints are introduced (eq. (13) and (14)), in order to enforce a reasonable combination of physical attributes. In addition to the laminate dependent design variables, the thickness of the planar elements is also a target of optimisation.

$$2V_1^2(1-V_3) + 2V_2^2(1+V_3) + V_3^2 + V_4^2 - 4V_1V_2V_4 \le 1$$
 (13)

$$V_1^2 + V_2^2 \le 1 \tag{14}$$

The material chosen for the wing box structure is *IM6* (Table 2). Its properties are publicly available in [14].

In order to account for material failure of carbon fibre laminates, a common approach during the optimisation is to define tensile (ε_t) , compressional (ε_c) and shear strain (γ) limits. Certain additional failure modes, like open hole strain peaks, are often accounted for by applying knock

down factors onto these limits, often resulting in highly conservative material restrictions.

| IM6 | |
|--|--------|
| Longitudinal Modulus (E_1 , GPa) | 177.0 |
| Transverse Modulus (E2, GPa) | 10.8 |
| Shear Modulus (G_{12} , GPa) | 7.6 |
| Poisson's Ratio (v_{12}) | 0.27 |
| Longitudinal Tensile Strength (X_t , MPa) | 2860.0 |
| Longitudinal Compressive Strength (X_c , MPa) | 1875.0 |
| Transverse Tensile Strength (Y_t , MPa) | 49.0 |
| Transverse Compressive Strength (Y_c , MPa) | 246.0 |
| Shear Strength (S, MPa) | 83.0 |

Table 2: Material Properties of IM6

As depicted in Table 3, the strain limits applied during optimisation are increased stepwise, until reaching a factor (s_F) of 3. This is done to gain a higher deflection of the wing and to answer the question of how the structural optimisation process changes by increasing strain level.

| Factor (s_F) | Strain Limits $(\varepsilon_t, \varepsilon_c, \gamma)$ | | | |
|----------------|--|------------|-------------|--|
| 1.00 | 2666.0 μs | -2333.0 μs | ±5333.0 μs | |
| 1.33 | 3467.0 μs | -3000.0 μs | ±6933.0 μs | |
| 1.66 | 4506.7 μs | -3858.0 μs | ±8533.0 μs | |
| 2.00 | 5333.0 μs | -4666.0 μs | ±10666.0 μs | |
| 2.50 | 6666.0 μs | -5832.5 μs | ±13333.0 μs | |
| 3.00 | 8000.0 μs | -7000.0 μs | ±16000.0 μs | |

Table 3: Strain Limits Applied in Structural Optimisation

Besides strain evaluation, intracell buckling of planar elements between stiffeners is considered following the engineering standards in [15]. According to this, the critical compressional buckling stress of a plate hinged at all 4 sides can be computed according to equation (15). This criterion is applied for elements belonging to the skins, whereas ribs and spars are checked against the critical shear stress calculated by equation (16). The parameters k_x and k_s depend on the clamping of the plate, its aspect ratio and the bending stiffness matrix \mathbf{D} . For a complete formulation refer to [15].

$$\mathbf{N}_{x,cr} = -k_x \left(\frac{\pi}{h}\right)^2 \left(\sqrt{D_{11}D_{22}}\right)$$
 (15)

$$\mathbf{N}_{xy,cr} = k_s \left(\frac{\pi}{b}\right)^2 \left(\sqrt{D_{11}D_{22}^3}\right)$$
 (16)

3.4.3. Beam Elements

Similar to the planar elements above, the stiffening elements feature a composition of CFRP. However, the only designed variable in this context is the height of their rectangular cross section. The fractional portions of plies are kept constant at (70% 0°, 20% ±45°, 10% 90°). Figure 8 depicts the division of the beam elements into design domains. These domains are arranged based on the

design fields presented in Figure 7. If beams are located at an intersection of plate design domains, an additional domain is created.

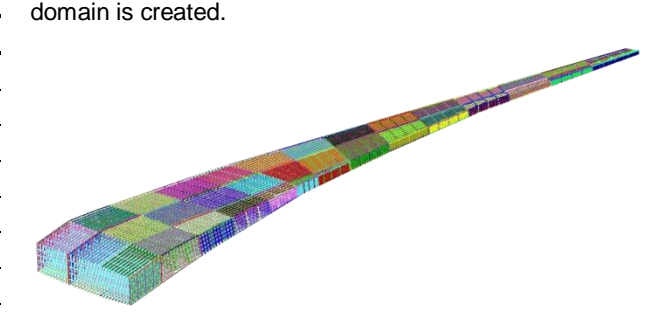


Figure 8: Visual Representation of Design Domains, Stiffening Elements

The optimisation of the stiffeners is constraint by strain limits, as well as by a semi empirical approach for beam column crippling. The applied strain limits are equal to the ones specified for the optimisation of the planar elements. Equations (17) and (18) represent the crippling constraint formulation taken from [16], in which the critical longitudinal crippling stress $F^{\rm cc}$ is formulated as a correlation between the ultimate longitudinal compression stress $F^{\rm cu}$ of the laminate, together with geometrical parameters of the web like the thickness t and height b, as well as laminate and ply-dependent values.

$$\frac{F^{cc}}{F^{cu}} \frac{E_x}{\overline{E}} = f \left(\frac{b}{t} \frac{\overline{E}}{E_x} \sqrt{\frac{F_{cu}}{\sqrt{E_x E_y}}} \right)$$
 (17)

$$\bar{E} = \frac{12D_{11}}{t^3} (1 - \nu_{xy} \nu_{yx}) \tag{18}$$

The calculated value is compared to the minor principal of the beam stress, while also including a safety margin of 1.5 in the calculation.

3.4.4. Linear Buckling Analysis

As strain limits are increased successively, the design is expected to become restricted by buckling of the stiffened panel as a whole. Therefore, linear buckling analyses are carried out during the optimisation phase. These analyses are not implemented separately, but rely on the routines available in MSC.NASTRAN itself. The governing equations described in the following are taken from [17] and [18]. In order to formulate a stability problem, a second order approach is pursued, accounting for higher order strain-displacement relationships in the element shape function. This leads to an additional differential stiffness term \mathbf{K}_d — also referred to as geometrical stiffness — which is dependent on the external load vector \mathbf{P} , but not on the displacement vector \mathbf{u} :

$$\mathbf{K} = \mathbf{K}_l + \mathbf{K}_d(\mathbf{P}). \tag{19}$$

In the case of a linear correlation between the geometrical stiffness and the external load, \mathbf{K}_d may be rewritten as:

$$\mathbf{K}_{d}(\mathbf{P}) = \mathbf{P}\overline{\mathbf{K}}_{d}.\tag{20}$$

Based on equations (19) and (20) the potential energy equation (eq. (21)) may be formulated and differentiated (eq. (22)). In case of a static equilibrium the change in potential energy \mathbf{U} has to become zero, which is fulfilled if the external load reaches a critical level \mathbf{P}_{cr} . As a consequence, equation (22) may be interpreted as an eigenvalue problem (eq. (23)).

$$\mathbf{U} = 0.5 \, \mathbf{u}^T \mathbf{K}_l \mathbf{u} + 0.5 \, \mathbf{u}^T \mathbf{K}_d \mathbf{u} \tag{21}$$

$$\frac{\partial \mathbf{U}}{\partial u} = \mathbf{K}_l u + \mathbf{K}_d u = \mathbf{0} \tag{22}$$

$$|[\mathbf{K}_l + \mathbf{P}_{cr_i} \overline{\mathbf{K}}_d]| \mathbf{u} = 0$$
 (23)

Since in this case the external load is independent of the displacement, it can be expressed as a product of the applied load P_a and a load factor λ_i .

$$P_{cr_i} = \lambda_i P_a \tag{24}$$

$$|[\mathbf{K}_l + \lambda_i \mathbf{K}_d]| u = \mathbf{0} \tag{25}$$

In the context of the presented structural optimisations the loads factors are constraint to be larger than 1.5. In the case of a structural certification it is adequate to verify that the lowest buckling load factor λ_1 is larger than 1.0 or a certain safety margin. However, as the buckling modes are subject to change during the optimisation, it becomes beneficial to calculate as many modes and their sensitivities regarding the design variables as possible. Throughout the design of the presented wing box model 85 buckling modes per load case are taken into account.

4. LOADS AND OPTIMISATION TOOL CHAIN

The tool chain depicted in Figure 9 is an adaption of the MoNa-process. MoNa is an acronym combining the most relevant tools of the design procedure: the in-house model ModGen and the structural generator MSC.NATRAN. The capabilities of this concept have been demonstrated in [19] and [20]. The tool chain itself is linked via python routines, increasing the modularity. In general, the process can be separated into two major segments. In a first step the estimation and generation of essential aircraft parameters is carried out (see chapter 2) and stored in a python object, representing the aircraft. Afterwards, this aircraft is passed to the each module of the structural optimisation phase. The latter is initiated with a Guan-reduction [21] in NASTRAN SOL101, reducing the degrees of freedom of the structural model. This is done to accelerate the loads calculations carried out in NASTRAN SOL144, which constitutes a static aeroelastic trim solver. After the loads are filtered, the remaining dimensioning loads are handed over to the structural optimisation of the full structure in NASTRAN SOL200. This process is repeated until convergence, while keeping the aircraft's total mass and centre of gravity constant through an adaption of the payload. If the objective is considered converged, the aircraft's aileron effectiveness, stability margin and tendency towards divergence are evaluated. This post processing step becomes necessary, since aircraft derivatives are currently not considered by the structural optimisation itself.

One enhancement of the presented version of the MoNaprocess is the bulk adaption before the structural optimiser, as well as a monitoring wrapped around the solver. Bulk adaption refers to changes made to the structural data set, like preparing the optimisation model of the beam elements or adding additional analyses like the linear buckling analysis. Additionally, the mesh of the structural model may be refined in order to enhance the quality of the buckling modes. Following [22], the module provides the possibility to aggregate the optimisation constraints based on the Kreiselmeier-Steinhauserformulation published in [23]. The latter procedure, however, has not been utilised for the design of the presented structural models, since the benefits in the reduction of computational resources are cancelled out by the overhead in the pre processing in MAC.NASTRAN.

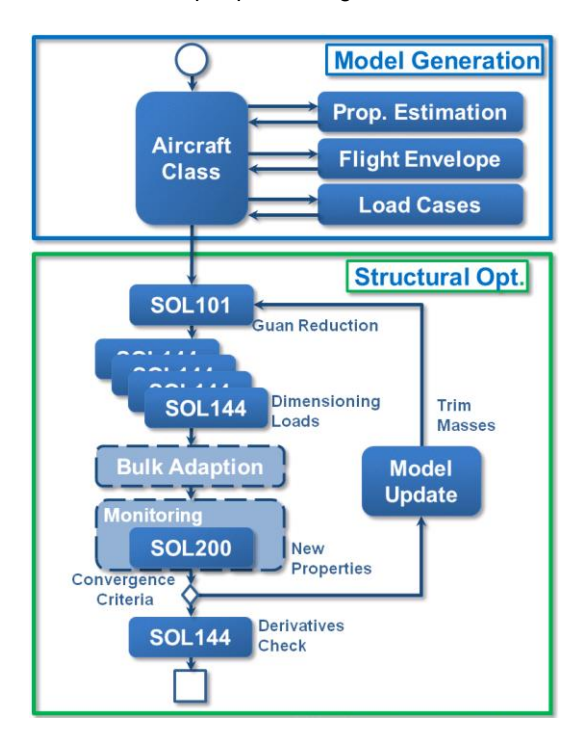


Figure 9: Tool Chain Flow Chart

The monitoring, on the other hand, becomes necessary due to the complexity of the optimisation problem, resulting in numerical errors while solving the optimisation problem. These errors are reproducible and may manifest in data base issues or numerical deadlocks. The latter describes a status in which the optimiser is restricted by conflicting constraints, unable to proceed in any direction. Only by pushing the design variables into the direction of a feasible design, like increasing plate thickness, the optimiser may overcomes this state.

One key advantage of the presented tool chain lies in its modularity. The source of the load, for example, is independent to the structural optimisation process. Furthermore, in the current configuration the linear load calculations allow for the computation and consideration of thousands of load cases. However, future research will have to investigate on whether it is critical to respect geometrically nonlinear effects during the load generation and structural optimisation. Furthermore, the lack of gust loads and the non-consideration of aerodynamic, flight dynamic or aeroelastic derivatives within the optimisation

is a shortcoming, which has to be resolved in future revisions of the process. In an attempt to ensure the pitching stability of the aircraft, the wing's torsion during design cruise flight is constraint to be smaller than 3.5°.

5. GEOMETRICALLY NONLINEAR FINITE ELEMENTS CALCULATIONS

6. RESULTS

In the following, several exemplary results of the design process and geometrically nonlinear finite element calculations are presented.

6.1. Optimisation

In order to determine the impact of varying stain limits on the optimisation process, two different objective functions are paired with increasing strain allowable factors listed in Table 3. The first function (eq. (2)) results in a pure maximisation of the vertical wing tip displacement during design cruise flight. This objective is from now on referred to as LD. The second objective uses equation (3) in combination with the exponents φ and ζ set to 1 and 2 respectively. The latter function will be referred to as WoD2.

Figure 10 depicts the convergence history of the WoD2 objective in combination with a strain limit factor (s_F) of 3.0. The relative maximum constraint (MRC) value represents the maximal violation of a constraint with respect to its bound. The objective features a steadily decreasing trend, while the MRC is diminished to a value from 0.1 to 0.005 %. This constitutes the desired convergence behaviour. Every red circle represents an update of the loads.

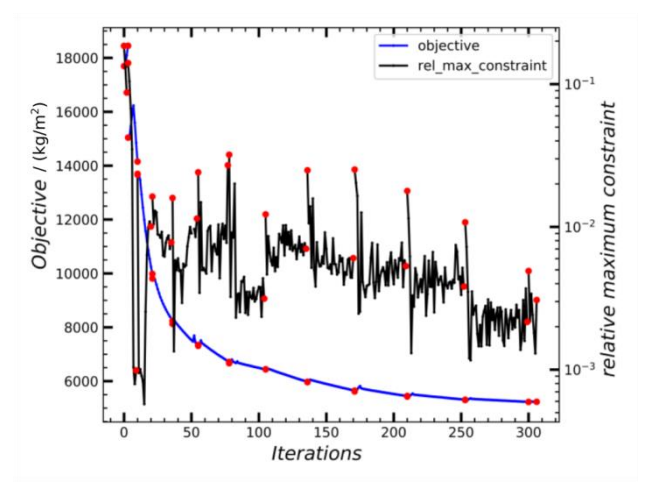


Figure 10: Optimisation Process Convergence History, Objective Function (3), φ =1, ζ =2, s_F =3.0

The resulting vertical wing tip displacements during design cruise flight, resulting from the parameter variation, are visualised in Figure 11. Both objectives feature a rising trajectory as the strain allowables are increased. However, the gradient diminishes for larger values of s_F . Furthermore, the overall difference between the two objectives remains rather small. This is especially noteworthy considering the trajectories of the mass

corresponding to the load carrying structure of the wing box (Figure 12).

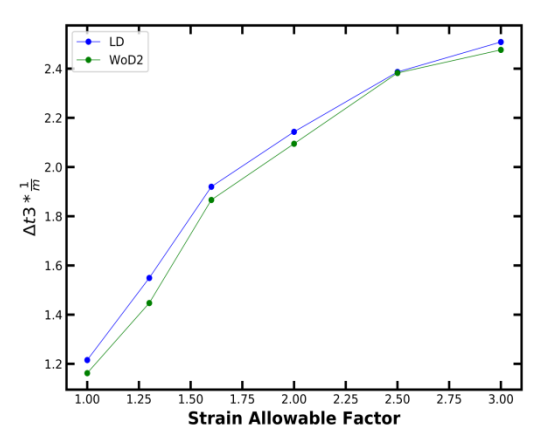


Figure 11: Linear Vertical Wing Tip Displacement in Design Cruise Flight plotted over Strain Limits

It becomes obvious that the small increase in deformation of the LD objective goes along with a massive weight penalty. The trend of the LD objective diminishes for a small increase of s_F , while becoming flat after a factor of 1.66. This change might be caused due to a weak linkage between deformation as an objective and structural mass in the optimisation. If the sensitivity of a design variable with respect to the deformation becomes zero, it will not be changed any further.

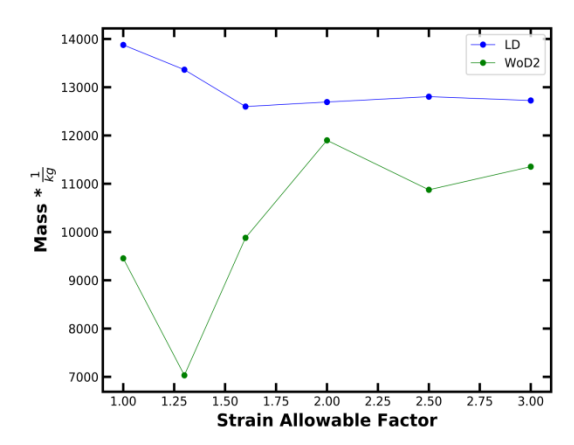


Figure 12: Mass of Load Carrying Wing Box Plotted over Strain Limits

Therefore, potential mass saving due to unused structure remains unutilised. On the other hand, studies of the constraints active during optimisation have shown that the kink in the mass slope goes along with a shift from strain to buckling being the limiting factor during optimisation. This might causes an increase in plate thickness and beam height to overcome this issue. The latter potentially explains the rising mass trajectory of the WoD2-objective after a strain limit factor of 1.33, since this behaviour seems rather unexpected. However, as the WoD2-objective is a weighted function its optima constitute a Pareto-surface. Therefore, the same objective value may be composed out of multiple combinations of the individual components. In order to properly evaluate the WoD2-trajecotry, one hast to compare it to a trend produced by

an objective solely minimising the structural mass, being object of future research.

Figure 13 visualises the stability margin of each individual design and emphasises the shortcomings of the current optimisation procedure. All of the performed optimisations lead to an instable design as their stability margin is negative.

Furthermore, the depicted slopes emphasise the large dependency of the aerodynamic neutral point on the deformation of the wing. This is expected, since the wing is swept back. If the outer wing twists forward during a coupled trim simulation, the overall lift distribution is shifted inwards.

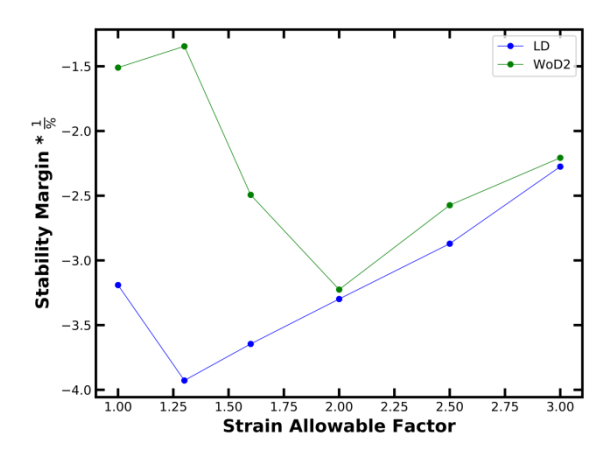


Figure 13: Stability Margin of the Aircraft Plotted over Strain Limits

In combination with the geometrical sweep the neutral point moves forward until it is finally placed in front of the centre of gravity, constituting an unstable state. The vastly changing stability margin emphasises that methodology of limiting the wing torsion to 3.5° during design cruise conditions is incapable of designing a stable aircraft. Consequently, the presented tool chain has to be altered to include such derivatives during the optimisation phase. Alternatively, one may extend the design process with additional variables, such as the position and size of the horizontal stabiliser. Another option could be the application of an active flight controller stabilising the aircraft. However, this concept is currently prohibited for use in civil passenger aircrafts.

6.2. Geometrically Nonlinear Calculations

This section presents the geometrically nonlinear finite element calculations carried out as a post processing step subsequent to the optimisation tool chain. These calculations are supposed to verify the integrity of the optimised structural model. Therefore, nonlinear static calculations are carried out in MSC.NASTRAN SOL400.

The governing equation can be formulated as in eq. (26). \mathbf{K}_t refers to the linear stiffness components, while the tangential stiffness matrix \mathbf{K}_t depends on the external load field and the displacement vector. Since the external load vectors of the linear trim calculations are recycled for this analysis, follower forces are neglected and \mathbf{P} becomes independent of \mathbf{u} .

$$\mathbf{K}_{t}\mathbf{u} + \mathbf{K}_{t}(\mathbf{P}, \mathbf{u})\mathbf{u} = \mathbf{P} \tag{26}$$

Consequently, this problem is solved by formulating a lagrangian approach, in which the external load field is scaled successively in multiple steps. Within each of these steps the problem is solved iteratively until the strain energy and the external work reach equilibrium. In order to account for large deformation effects and element offsets in the generation of the tangential stiffness matrix, one has to specifically activate those features in MSC.NASTRAN. Furthermore, it is necessary to convert linear elements, like rods or bars, to equivalents featuring a nonlinear formulation. If the structure suffers from buckling, the iteration procedure during the employed Lagrangian approach is likely to diverge, rendering the model unusable for further research.

In the current context, the calculations are carried out using the wing model obtained by employing the WoD2-objective in combination with a strain limit factor of 3.0. The applied load fields are extracted from linear trim calculations. Table 4 lists the defined flight conditions. Throughout all of the calculations the wing attachment is fixed in a clamping.

| Manoeuvre | n_z / g | Ма | $q / \frac{N}{m^2}$ | Mass Config. |
|--------------|-----------|-------|---------------------|--------------|
| pull up | 2.5 | 0.514 | 18738.00 | MTAYed |
| level flight | 1.0 | 0.85 | 12058.44 | MTAYed |
| push down | -1.0 | 0.514 | 18738.00 | MTAYed |

Table 4: Manoeuvre Flight Conditions

Figure 14 depicts the results of the geometrically nonlinear calculations. When applying the loads fields obtained from a linear level flight (1.0g), the deflection reaches a value of 8.5% with respect to the wing half span. Especially when considering the results of the 2.5g and -1.0g load cases, the necessity for geometrically nonlinear calculations becomes apparent. In contrast to linear calculations, the overall length of the wing, and therefore the lifting surface, is preserved. The quantification of the latter effect and its impact on the dimensioning loads is topic of future research.

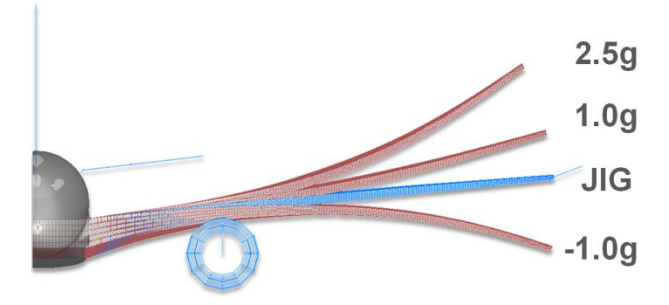


Figure 14: Geometrically Nonlinear Deflections of Optimised Wing Structure

7. CONCLUSION

The presented work emphasises the extensive effort one has to undergo in order to design a highly flexible wing box structure for a civil passenger aircraft. A

comprehensive simulation model of a long range jet transport was developed, featuring all the necessary components in order to calculate manoeuvre loads and optimise the load carrying wing box structure. Furthermore, a tool chain was developed, automating the whole process of defining a flight envelope, generating load cases, calculating loads, optimising the structure and updating the model. Based on this framework, a highly flexible carbon fibre wing box structure was designed. This was achieved by employing a lamination parameter based optimisation and increasing the strain limit factors.

As the flexibility of the structure rises, buckling failure modes become a limiting factor within the optimisation. Therefore, topological decisions and analytical measures with the objective of avoiding buckling failures have been illustrated. The resulting most flexible wing structure features a vertical tip displacement in design cruise flight of 8.5 % with respect to half span. It has been shown, that the increase in strain limits results in a significant raise in deformation. However, for the considered objective functions the mass does not follow a predictable trend. The evaluation of the mass trajectories has proven to be difficult due to the lack of comparable data generated exclusively with the objective of minimising the structural mass. The latter is missing since it turned out to be converging poorly. It is uncertain whether the fluctuation in the WoD2 trend is caused due to the formulation of a Pareto surface as an optimum or if the rise in mass is the result of increased buckling limitations. Further evaluation of this matter will be part of future research.

The assessment of the stability margin revealed issues with the pitching stability. This is caused by a large movement of the aircraft's neutral point. As a consequence, the process will be altered to account for stability derivatives during the structural optimisation.

Additionally to the structural design, geometrically nonlinear calculations were performed to verify the suitability of the model for such analyses. These calculations emphasise the necessity of accounting for structural nonlinearities for highly flexible structures. Consequently, future research will focus on developing a geometrically nonlinear loads process. This process, together with the presented simulation model, will provide the possibility to quantify the differences resulting from geometrically linear and nonlinear trim calculation.

References

- [1] S. Sengupta, "New York Times," 20 September 2019. [Online]. Available: https://www.nytimes.com/2019/09/20/climate/globa l-climate-strike.html. [Accessed 24 September 2019].
- [2] P. D. W. R. Krüger, "Technologien zur Analyse und Reduktion von Lasten an Verkehrsflugzeugen (ATLAS2Hybrid/ReduLa): Schlussbericht.," 2018, Available: https://elib.dlr.de/126449/
- [3] European Aviation Safety Agency, Certification Specifications and Acceptable Means of Compliance for Large Aeroplanes, CS-25, Amendment 23, Subpart B and C, 2019.

- [4] A. Bérard and A. T. Isikveren, "Conceptual Design Prediction of the Buffet Envelope of Transport Aircraft," *Journal of Aircraft* vol. 46, no. 5, 2009.
- [5] T. Klimmek, "Parametric Set-Up of a Structural Model for FER-MAT Configuration for Aeroelastic and Loads Analysis.," *Journal of Aeroelasticity and Structural Dynamics*, no. 3.2, pp. 31-49, May 2014.
- [6] T. Klimmek, "Statische aeroelastische Anforderungen beim multidisziplinären Strukturentwurf von Transportflugzeugflügeln," Göttingen, 2016, dissertaition, Technical University of Braunschweig
- [7] E. Torenbeek, Development and application of a comprehensive, design-sensitive weight prediction method for wing structures of transport category aircraft, Delft: Technical University of Delft, 1992.
- [8] F. Dorbath and L. v. Veen, "Wing Secondary Structure Statistical Mass Estimation," in *Luftfahrttechnisches Handbuch*, Ottobrunn, IAB GmbH, 2012.
- [9] MSC Software, "MSC Nastran 2017 Aeroelastic User's Guide (SOL144)," 28 November 2016. [Online]. Available: https://simcompanion.mscsoftware.com/infocenter/index?page=content&id=DOC11570&cat=MSC_NASTRAN_DOCUMENTATION_2017&actp=LIST. [Accessed 03 July 2019].
- [10] A. Wächter and L. T. Biegler, "On the implementation of an interior-point filter line-search algorithm for large-scale nonlinear programming," *Mathematical Programming*, vol. 106, no. 1, pp. 25-57, March 2006.
- [11] S. Tsai and N. Pagano, "Invariant Properties of Composite Materials," Defense Technical Information Center, 1968.
- [12] V. Hammer, M. Bendsøe, R. Lipton and P. Pedersen, "Parametrization in laminate design for optimal compliance," *International Journal of Solids and Structures*, vol. 34, no. 4, pp. 415-434, February 1997.
- [13] S. Setoodeh, M. Abdalla and Z. Gürdal, "11th AIAA/ISSMO Multidisciplinary Analysis and Optimization Conference," in *Approximate Feasible Regions for Lamination Parameters*, Portsmouth, Virginia, 2006.
- [14] I. M. Daniel and O. Ishai, "Engineering Mechanics of Composite Material," Oxford University Press In., Oxford, 1994.
- [15] Verein Deutsche Ingenieure e.V., "Development of FRP components, Analysis," in *VDI 2014*, vol. 3, 2006.
- [16] Department of Defense, Composite Materials Handbook, vol. 3., 2002, USA
- [17] MSC-Software, *Linear Static User's Guide*, 2017, pp. 523-526.

- [18] M. Link, Finite Elemente in der Statik und Dynamik, 4. ed., Springer Verlag, 2014, pp. 97-103.
- [19] J. Dillinger, Static Aeroelastic Optimization of Composite Wings with Variable Stiffness Laminates, Delft University of Technology, 2014.
- [20] K. Bramsiepe, V. Handojo, Y. Meddaikar, M. Schulze and T. Klimmek, "Loads and Struktural Optimization Process for Composite Long Range Transport Aircraft Configuration," in *Multidisciplinary Analysis and Optimization Conference*, Georgia, Atlanta, 2018.
- [21] R. J. Guyan, "Reduction of Stiffness and Mass Matrices," *AIAA Journal*, vol. 3, no. 2, p. 380, 1965.
- [22] G. A. Wrenn, "An Indirect Method for Numerical Optimization Using the Kreisselmeier-Steinhauser Function, NASA Contractor Report 4220," 1989.
- [23] Kreiselmeier, G.; Steinhauser, R.;, "International Federation of Acitve Controls Symposium on Computer-Aided Design of Control Systems," in *Systematic Control Design by Optimizing a Vectro Performance Index*, Zurich, 1979.